Cell Reports

Structural Basis for EPC1-Mediated Recruitment of MBTD1 into the NuA4/TIP60 Acetyltransferase Complex

Graphical Abstract

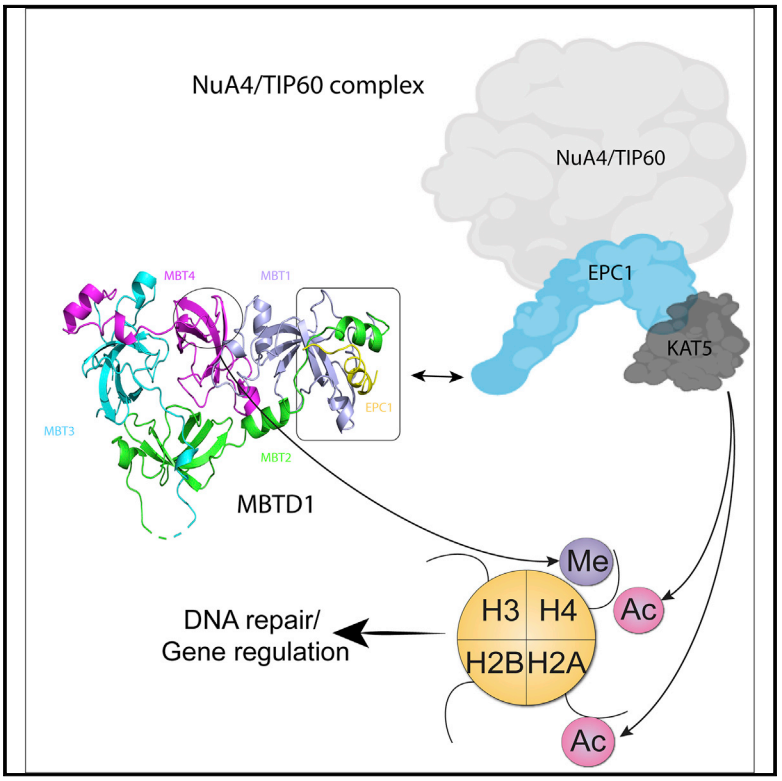

Highlights

- The crystal structure of EPC1 bound to MBTD1 is determined
- MBTD1 employs two distinct regions to recognize H4K20me and EPC1
- Mutations at the MBTD1-EPC1 interface affect gene expression and DNA repair

Authors

Heng Zhang, Maëva Devoucoux, Xiaosheng Song, ..., Peter Loppnau, Jacques Côté, Jinrong Min

Correspondence

jacques.cote@crhdq.ulaval.ca (J.C.), jr.min@utoronto.ca (J.M.)

In Brief

EPC1 is a critical component of the NuA4/TIP60 acetyltransferase complex involved in gene expression and genome maintenance. Zhang et al. illuminate the structural and molecular basis for EPC1 bound to the H4K20me reader MBTD1, highlighting the important role of their association in gene transcription and DNA repair.

Zhang et al., 2020, Cell Reports *30*, 3996–4002
March 24, 2020
https://doi.org/10.1016/j.celrep.2020.03.003

CellPress

OPEN ACCESS
CellPress

Cell Reports
Report

Structural Basis for EPC1-Mediated Recruitment of MBTD1 into the NuA4/TIP60 Acetyltransferase Complex

Heng Zhang,[1,6] Maëva Devoucoux,[2,6] Xiaosheng Song,[1] Li Li,[1] Gamze Ayaz,[1,3] Harry Cheng,[1] Wolfram Tempel,[1] Cheng Dong,[1] Peter Loppnau,[1] Jacques Côté,[2,*] and Jinrong Min[4,5,7,*]

[1]Structural Genomics Consortium, University of Toronto, Toronto, ON M5G 1L7, Canada
[2]St. Patrick Research Group in Basic Oncology, Laval University Cancer Research Center, Oncology division of CHU de Québec-Université Laval Research Center, Quebec City, QC G1R 3S3, Canada
[3]Department of Biology, Middle East Technical University, Ankara, Turkey
[4]Hubei Key Laboratory of Genetic Regulation and Integrative Biology, School of Life Sciences, Central China Normal University, Wuhan 430079, PR China
[5]Structural Genomics Consortium and Department of Physiology, University of Toronto, Toronto, ON M5S 1A8, Canada
[6]These authors contributed equally
[7]Lead Contact
*Correspondence: jacques.cote@crhdq.ulaval.ca (J.C.), jr.min@utoronto.ca (J.M.)
https://doi.org/10.1016/j.celrep.2020.03.003

SUMMARY

MBTD1, a H4K20me reader, has recently been identified as a component of the NuA4/TIP60 acetyltransferase complex, regulating gene expression and DNA repair. NuA4/TIP60 inhibits 53BP1 binding to chromatin through recognition of the H4K20me mark by MBTD1 and acetylation of H2AK15, blocking the ubiquitination mark required for 53BP1 localization at DNA breaks. The NuA4/TIP60 non-catalytic subunit EPC1 enlists MBTD1 into the complex, but the detailed molecular mechanism remains incompletely explored. Here, we present the crystal structure of the MBTD1-EPC1 complex, revealing a hydrophobic C-terminal fragment of EPC1 engaging the MBT repeats of MBTD1 in a site distinct from the H4K20me binding site. Different cellular assays validate the physiological significance of the key residues involved in the MBTD1-EPC1 interaction. Our study provides a structural framework for understanding the mechanism by which MBTD1 recruits the NuA4/TIP60 acetyltransferase complex to influence transcription and DNA repair pathway choice.

INTRODUCTION

Coordination of posttranslational modifications (PTMs) represents an important signaling mechanism to control often-complex biological processes such as DNA repair (Chin, 2017; Dantuma and van Attikum, 2016; Woodsmith et al., 2013; Woodsmith and Stelzl, 2014). DNA double-strand break (DSB) is one of the most severe forms of genomic lesions whose improper repairs will trigger genomic instability and lead to malignant transformation (Hustedt and Durocher, 2016; Pommier et al., 2016; Wilson and Durocher, 2017). To properly repair these dangerous genetic lesions, mammalian cells have evolved complex yet highly orchestrated signaling cascades involving various PTMs such as ubiquitylation, methylation, and acetylation for context-dependent signal propagation. The NuA4 (Nucleosome Acetyltransferase of H4)/TIP60 (Tat Interacting Protein 60) acetyltransferase complex has been demonstrated to participate in the repair of DNA DSBs at multiple levels, underlining the pleiotropic contributions of acetylation as a PTM to the DNA DSB repair network (Dhar et al., 2017; Jacquet et al., 2016; Paquin and Howlett, 2018; Rossetto et al., 2010; Soria et al., 2012; Tang et al., 2013).

Two major pathways exist to repair DNA DSBs in mammalian cells, namely, homologous recombination (HR) and non-homologous end joining (NHEJ) (Her and Bunting, 2018; Sunada et al., 2018). The choice between these two canonical DSB repair pathways often determines the cellular fate post-DNA damage and can have significant implications for related human syndromes, as well as therapeutic strategies (Chapman et al., 2012; Liu et al., 2016; Sung, 2018). The recruitment and retention of 53BP1 has been suggested to potentiate NHEJ-mediated repair of DSBs primarily by safeguarding DSB ends from DNA end resection, a key requirement to initiate HR-mediated repair (Gupta et al., 2014; Liu and Huang, 2016). Although 53BP1 can be recruited to the DSB sites partly by binding to the H4K20me mark, RNF168-mediated mono-ubiquitination on H2AK13/15 is also key to the 53BP1 appearance at the break, leading to the DSB being repaired through the error-prone NHEJ pathway (Fradet-Turcotte et al., 2013; Zimmermann and de Lange, 2014). Another H4K20me reader protein, MBTD1 (malignant brain tumor [MBT] domain-containing protein 1), has recently been demonstrated to be a stable subunit of the NuA4/TIP60 acetyltransferase complex (Jacquet et al., 2016). Interestingly, MBTD1 affects the recruitment of the NuA4/TIP60 complex to a specific subset of genes to regulate their expressions (Jacquet et al., 2016). NuA4/TIP60-associated MBTD1 binding to the H4K20me mark at DSB sites competes with 53BP1 for association with the chromatin surrounding the lesion (Jacquet et al., 2016). The MBTD1-linked Tip60/KAT5(lysine acetyltransferase 5) enzyme catalyzes acetylation of not only the histone H4 tail, destabilizing 53BP1 interaction (Tang et al., 2013), but also H2AK15 to prevent its ubiquitylation by RNF168,

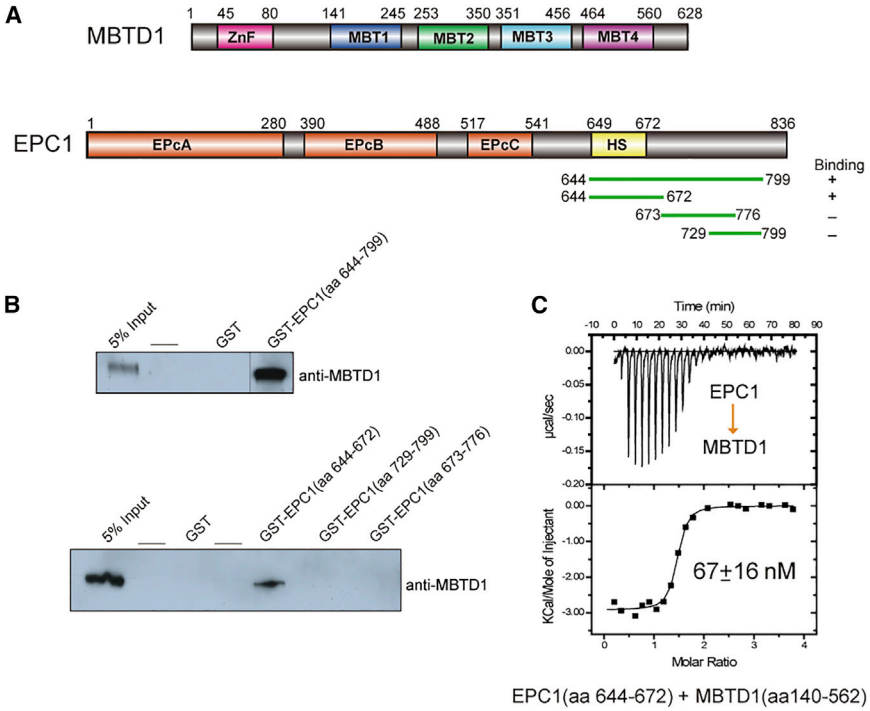

Figure 1. Characterization of the MBTD1-EPC1 Interaction

(A) Schematic domain organization of MBTD1 and EPC1. EPc, Enhancer of Polycomb; HS, hydrophobic segment; ZnF, zinc finger. (Right bottom) The truncated EPC1 proteins (green lines) used for GST pull-down are labeled with residue numbers.

(B) Western blot analysis of GST pull-down using His-MBTD1 incubated with the indicated GST-tagged EPC1 fragments. The amounts of GST-tagged EPC1 proteins used were normalized by Coomassie staining (Figure S1).

(C) Binding of EPC1 to MBTD1 was measured with ITC. The N value is ~1.3. The GST-EPC1 protein was titrated against the MBTD1 protein.

See also Figure S1.

thereby blocking the recruitment and retention of 53BP1 to the DSB sites (Jacquet et al., 2016). Collectively, MBTD1 via its direct interaction with the EPC1 (enhancer of polycomb homolog 1) subunit of the NuA4/TIP60 acetyltransferase complex negatively regulates 53BP1's bivalent associations with chromatin surrounding DSB sites through competition for binding to H4K20me and histone lysine acetylation (Jacquet et al., 2016). Therefore, this MBTD1-EPC1 interaction not only regulates certain gene expressions but also enables the recruitment of the DNA end resection machinery to the DSB site and commits the cellular response to the error-free HR pathway.

MBTD1 consists of a N-terminal FCS (named after the signature phe-cys-ser residues) zinc finger that binds to regulatory RNAs and four MBT domains that recognize the H4K20me1/me2 mark (Eryilmaz et al., 2009; Lechtenberg et al., 2009). The first and second MBT domains are reported to accommodate transcription factor YY1 *in vitro* (Alfieri et al., 2013), whereas the fourth MBT domain harboring the semi-aromatic cage is responsible for histone mark readout (Eryilmaz et al., 2009). EPC1 contains EPcA, EpcB, and EPcC domains at the N terminus (Kee et al., 2007). The C terminus of EPC1 was reported to interact with transcriptional repressor RFP (ret finger protein) (Tezel et al., 2002). The precise molecular mechanism by which MBTD1 associates with EPC1 remains elusive. Through structural analysis coupled with biophysical and functional analysis, we have elucidated the interaction mechanism between MBTD1 and EPC1-containing NuA4/TIP60 acetyltransferase complex. Hence, these data will provide information for the development of inhibitors for dissociating TIP60 acetyltransferase from the DSB sites and thereby enable the manipulation of DSB repair pathway choice, which can have clinical implications.

RESULTS AND DISCUSSION

Characterization of the Key EPC1 Region Responsible for Binding to MBTD1

MBTD1 has been recently revealed to associate with the NuA4/TIP60 acetyltransferase complex via its interaction with the C terminus of EPC1, a non-catalytic subunit of the core complex (Jacquet et al., 2016). To investigate the detailed molecular mechanism behind the MBTD1-mediated recruitment of the NuA4/TIP60 acetyltransferase complex to chromatin, we first aimed to narrow down the key region on the C terminus of EPC1 (Figure 1A). We performed *in vitro* glutathione S-transferase (GST) pull-down experiments followed by western blot. GST-EPC1$^{644–799}$ efficiently bound MBTD1, whereas GST-EPC1$^{729–799}$ and GST-EPC1$^{673–776}$ lacking a hydrophobic region did not (Figures 1A, 1B, and S1), suggesting that this hydrophobic fragment (residues 644–672) of EPC1 is likely responsible for binding of MBTD1. Indeed, the GST-EPC1$^{644–672}$ fragment was able to pull down MBTD1 (Figure 1B). Further isothermal titration calorimetry (ITC) studies confirmed that EPC1$^{644–672}$ directly interacts with MBTD1 with a dissociation constant (K_D) of ~67 nM (Figure 1C), indicating that the hydrophobic C-terminal fragment of EPC1 (residues 644–672) enlists MBTD1 into the dynamic NuA4/TIP60 acetyltransferase complex (Figure 1A).

Overall Structure of the MBTD1-EPC1 Complex

To elucidate how the NuA4/TIP60 acetyltransferase complex engages MBTD1 at the atomic level, we determined the crystal structure of MBTD1$^{140–562}$ in complex with EPC1$^{644–672}$ (Table S1). The well-defined electron density allowed us to build residues Lys649-Thr665 of EPC1 and all four MBT domains (MBT1–MBT4) of MBTD1 (Figure 2A). Intriguingly, EPC1 folds into a helical structure that locks into a hydrophobic binding groove formed by the MBT1 and MBT2 repeats of MBTD1 (Figure 2B), indicating that hydrophobic intermolecular interactions dictate the recruitment of MBTD1 into the NuA4/TIP60 acetyltransferase complex. Specifically, two

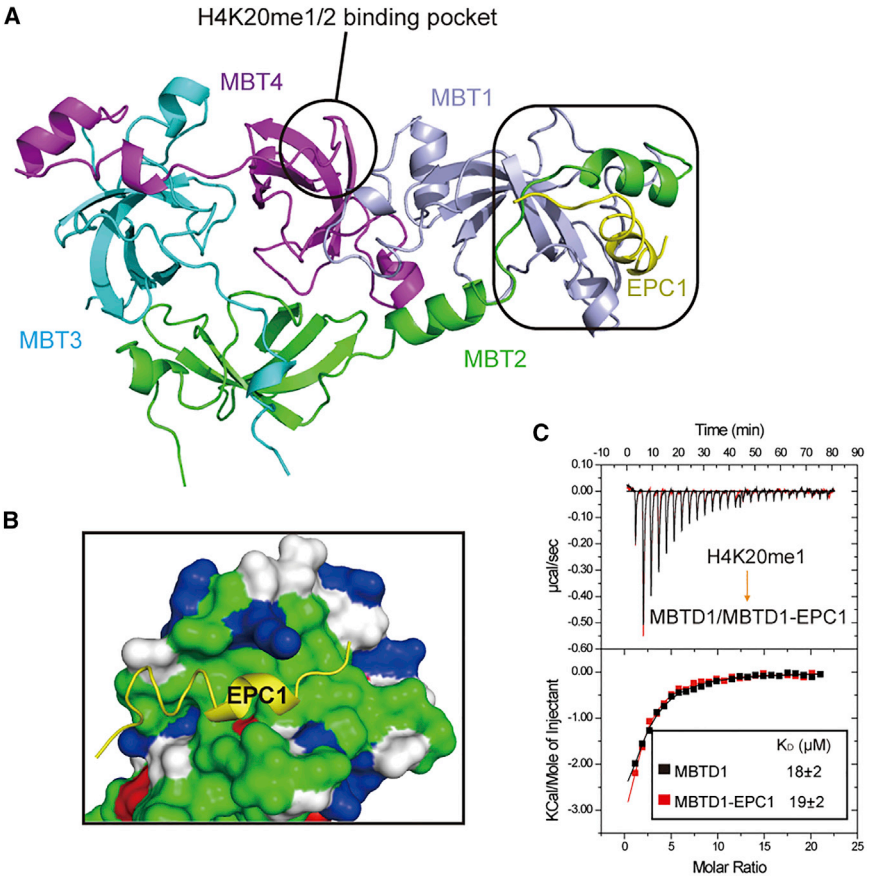

Figure 2. Crystal Structure of EPC1 Bound to MBTD1

(A) Overall structure of MBTD1 in complex with EPC1. The color scheme is the same as in Figure 1A.

(B) Surface representation of MBTD1 showing the hydrophobic pockets for binding of EPC1. Nonpolar residues of MBTD1 are colored green, polar residues are gray, positively charged residues are blue, and negatively charged residues are red.

(C) ITC titration curves of H4K20me1 (sequence: AKRHRKmeVLRDN) to MBTD1 (black curve) or the MBTD1-EPC1 complex (red curve).

See also Figure S2 and Table S1.

helices from MBT1 and MBT2 form a V-shaped groove (hereafter named the helical groove) to anchor EPC1. The overall structure of MBTD1 in the complex is highly similar to the previously determined apo structure (PDB: 3FEO) with an root-mean-square deviation (RMSD) value of approximately 0.36 Å (Figure S2A) (Eryilmaz et al., 2009). However, subtle structural divergences are observed in the hydrophobic helical groove of MBTD1 between the apo and the MBTD1-EPC1 complex structures. The binding of EPC1 triggers a mild yet significant displacement of the hydrophobic helical groove of MBTD1 compared with the apo structure, especially residues I229-V243, resulting in a relatively more open hydrophobic binding groove upon EPC1 lock-in (Figure S2B). The hydrophobic helical groove in the apo structure of MBTD1 has a high B-factor value, whereas it is well ordered in the complex structure, indicating that the EPC1 binding event can stabilize the hydrophobic helical groove of MBTD1 (Figure S2C). Given that (1) only the MBT4 repeat of MBTD1 contains the semi-aromatic cage to recognize H4K20me (Eryilmaz et al., 2009), (2) EPC1 binding does not involve the MBT4 repeat, and (3) this binding event does not induce significant conformational change on the MBT4 repeat structure, it is unlikely that the MBTD1-EPC1 interaction would affect MBTD1's binding ability toward H4K20me (Figure 2A). Consistently, our biophysical analysis demonstrated that MBTD1 displayed similar binding affinities toward H4K20me1 in the presence or absence of EPC1 (Figure 2C). Collectively, the preceding data suggest that the association of MBTD1 with the NuA4/TIP60 core complex does not impair its H4K20me binding ability, thereby conferring this histone mark binding capability to the NuA4/TIP60 acetyltransferase complex and influencing transcription and the DNA repair pathway choice.

Recognition Mechanism of EPC1 by MBTD1

In the complex structure, EPC1 exhibits an extended conformation and is sandwiched between two helices of MBTD1 (Figure 2B). Two hydrophobic leucine residues (Leu651 and Leu663) of EPC1 fit snugly into two separate hydrophobic pockets in MBTD1, respectively (Figure 3A). Specifically, Leu663 located at the C terminus of EPC1 occupies the hydrophobic cleft formed by Trp193, Pro244, Trp255, and Leu259 of MBTD1 (Figure 3A). Leu651 from the N terminus of EPC1 forms hydrophobic interactions with Val232, Leu263, and Ala266 of MBTD1. Similarly, at the center of the binding interface, Ala660 is accommodated by a hydrophobic patch created by Leu259, Val260, and Leu263 of MBTD1. Ala656, Phe658, and Ala662 of EPC1 also made hydrophobic interactions with their respective neighboring residues of MBTD1 (Figure 3A). In addition to the hydrophobic contacts, hydrogen bonds mediate the intermolecular interactions, strengthening their association. In particular, the main chain of Leu651 from the N terminus of EPC1 engages in hydrogen bonds with the main chains of Gly265 and Ala266. At the C terminus of EPC1, Ala662 and Val664 establish hydrogen bonds with Leu242. Moreover, Ala659 in the middle of EPC1 forms water-mediated hydrogen bonds with Glu179 and Ala236 (Figure S2F). These residues involved in the binding of EPC1 with MBTD1 are largely conserved across different species (Figures 3B and 3C), suggesting an evolutionarily conserved recognition mechanism of EPC1 by MBTD1. Altogether, the combined hydrophobic and polar intermolecular interactions are the major driving forces to enlist MBTD1 via EPC1 into the NuA4/TIP60 core complex.

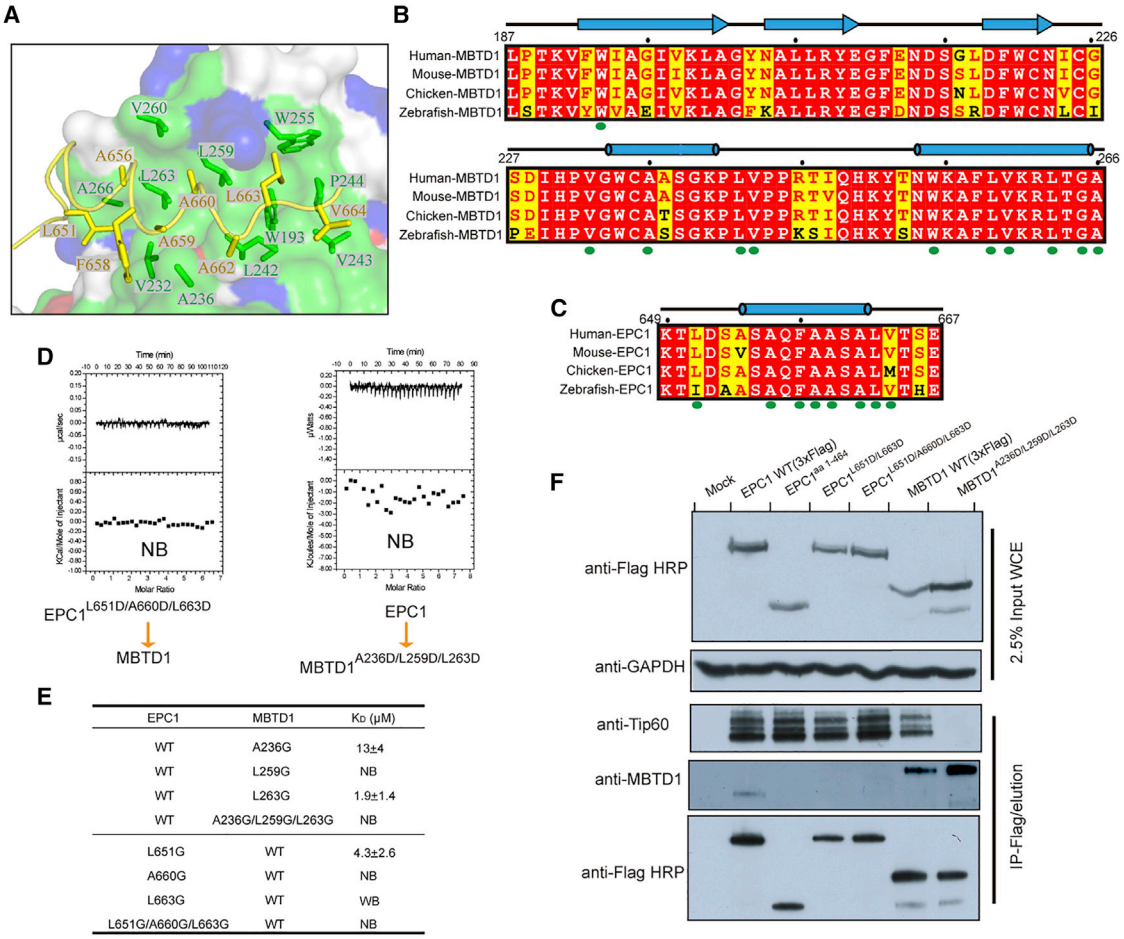

Figure 3. Recognition Mechanism of EPC1 by MBTD1

(A) Detailed interactions of MBTD1 with EPC1. The residues involved in the interactions are shown in stick representations, with the same color scheme as in Figure 2B.

(B) Sequence alignment of the helical groove regions of four MBTD1 orthologs. Green circles indicate the residues involved in the MBTD1-EPC1 interactions.

(C) Sequence alignment of the MBTD1 binding region of five EPC1 orthologs.

(D) Thermodynamic analysis of the interaction between EPC1 triple mutation and MBTD1 (left) and EPC1 and MBTD1 triple mutation (right). NB, no detectable binding.

(E) Quantification of the binding affinity between indicated EPC1 and MBTD1 by ITC. NB, no detectable binding; WB, weak binding.

(F) K562 isogenic cell lines stably expressing 3×FLAG-tagged EPC1 or 3×FLAG-tagged MBTD1 with the indicated mutations from the AAVS1 locus. Complexes were immunoprecipitated with anti-FLAG antibody, eluted with FLAG peptides, and analyzed by western blotting with the indicated antibodies.

See also Figures S2 and S3.

Structural Comparison of the MBTD1-EPC1 and MBTD1-YY1 Complexes

Given that the transcription factor YY1 has been previously demonstrated to directly bind to MBTD1 *in vitro* (Alfieri et al., 2013), we sought to compare the recognition mechanisms of YY1 and EPC1 by MBTD1. Interestingly, MBTD1 employs the same helical groove to capture both EPC1 and YY1, suggesting a conserved scaffold role of the helical groove in the assembly of MBTD1-associated protein complexes (Figure S2D). However, substantial structural differences are observed between MBTD1-EPC1 and MBTD1-YY1. EPC1 folds into a short helix in the MBTD1-EPC1 complex, whereas YY1 adopts a two-stranded β sheet in the MBTD1-YY1 complex (Figure S2D). Furthermore, both the helical groove and YY1 have higher B-factor values compared with those in the MBTD1-EPC1 complex (Figure S2C), indicating the flexibility of YY1. Consistently, a weaker binding affinity has been reported between YY1 and MBTD1 in the micro-molar affinity range, and no detectable binding has been observed between YY1 and MBTD1 *in vivo* (Alfieri et al., 2013; Jacquet et al., 2016). Although MBTD1 binds both EPC1 and YY1 predominantly through hydrophobic interactions, several key EPC1 binding residues of MBTD1 (Trp193, Ala236, Val243, and Trp255) are not involved in YY1 binding (Figure S2E). Point mutations of these residues significantly impaired the MBTD1-EPC1 association (Figures 3E and S3). Hence, the absence of these hydrophobic interactions in the MBTD1-YY1 might explain why MBTD1 displays weaker binding to YY1.

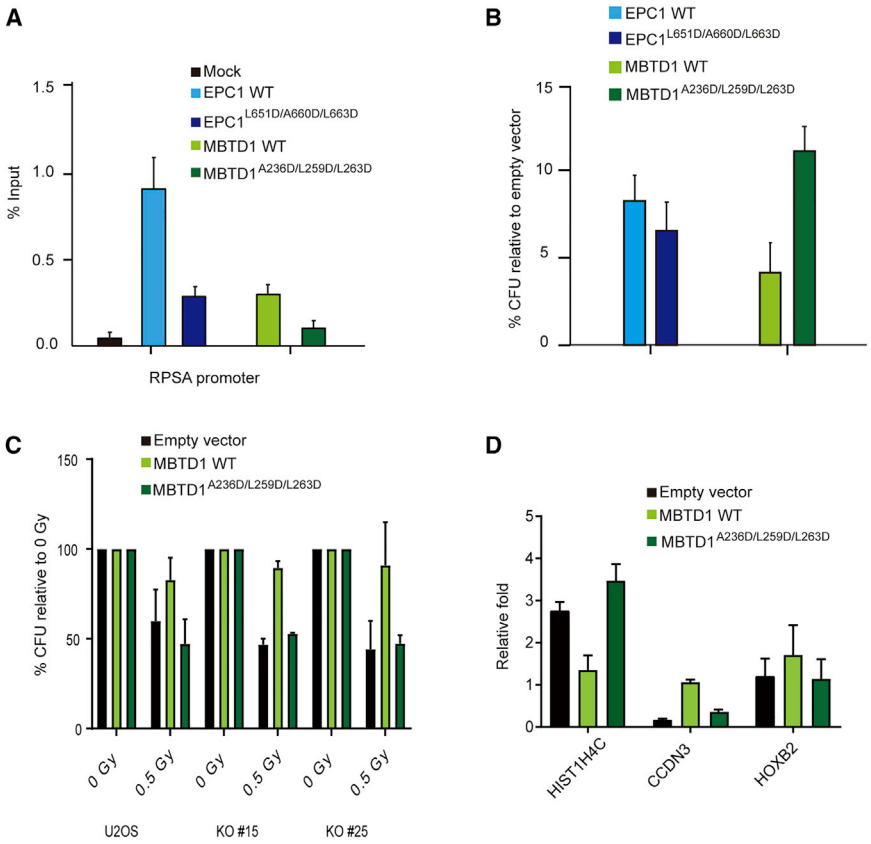

Figure 4. Interaction of MBTD1 and EPC1 Affects Gene Regulation, DNA Damage Response, and Cell Growth

(A) MBTD1 or EPC1 mutants affect recruitment to a target gene *in vivo*. ChIP was performed using K562 cells stably expressing MBTD1 or EPC1 mutant proteins. Error bars represent the range of two independent experiments.

(B) Clonogenic assay using U2OS cells transfected with the indicated expression vectors or empty vectors.

(C) WT MBTD1, but not the EPC1 binding mutant, suppresses the DNA damage sensitivity of MBTD1 knockout (KO) cells. Clonogenic survival assay showing the percentages of viable colonies for each condition after a single dose of gamma irradiation (0.5 Gy) relative to their respective untreated controls.

(D) WT MBTD1, but not the EPC1 binding mutant, complements the gene regulation defects in MBTD1 KO cells. Expression levels of genes that are dysregulated in MBTD1 KO cells (Jacquet et al., 2016), as measured by qRT-PCR 48 h posttransfection after transfection with empty vector, WT MBTD1, or MBTD1$^{A236D/L259D/L263D}$. WT and mutant MBTD1 are expressed to similar levels in this experiment (Figure S4D).

See also Figure S4.

Mutational Analyses Identified Some Key Residues Involved in the MBTD1-EPC1 Interaction

To validate the importance of the residues involved in the MBTD1-EPC1 interaction, we introduced point mutations of some key residues into MBTD1 and EPC1 and tested their binding affinities by ITC. Our structural analysis shows that Leu651, Ala660, and Leu663 of EPC1 are involved in hydrophobic interactions with MBTD1, suggesting an important role of these residues in the complex formation. Consistently, the triple-mutant EPC1$^{L651D/A660/L663D}$ abolished its binding to MBTD1 (Figure 3D). Similarly, the aspartic acid substitutions of the key residues of MBTD1 (MBTD1$^{A236D/L259D/L263D}$), identified from the MBTD1-EPC1 complex structure, impaired MBTD1-EPC1 association (Figure 3D). Furthermore, GST pull-down assays showed that the aspartic acid substitutions of some other key residues in the MBTD1-EPC1 interface significantly dampened complex formation (Figures S3A and S3B). To further discern the residues critical for MBTD1-EPC1 association, we generated glycine substitutions for both EPC1 and MBTD1 proteins. Our ITC data showed that single-glycine substitutions of hydrophobic residues significantly reduced or disrupted MBTD1-EPC1 binding (Figures 3E and S3C). Triple-glycine mutations abolished the interactions between EPC1 and MBTD1, which is consistent with aspartic acid substitutions. Collectively, our mutagenesis analysis confirmed the importance of the key residues involved in the hydrophobic interactions between MBTD1 and EPC1 in leashing MBTD1 to the NuA4/TIP60 complex.

To further examine the impacts of the key EPC1 mutations on their abilities to associate with MBTD1 *in vivo*, we generated isogenic K562 cell lines with a single copy of the epitope-tagged EPC1 gene inserted at the *AAVS1* safe-harbor locus as described previously (Jacquet et al., 2016). As expected, a C-terminal deletion mutant of EPC1 (EPC1$^{1–464}$) lost its ability to associate with MBTD1 in cells (Figure 3F). In accordance with the preceding ITC results, the triple-mutant EPC1$^{L651D/A660D/L663D}$ showed complete loss of co-purification with MBTD1 but retained association with Tip60 *in vivo* (Figure 3F). Similar experiments with K562 cell lines expressing epitope-tagged MBTD1 confirmed that residues Ala236, Leu259, and Leu263 of MBTD1 are fundamental to MBTD1's ability to associate with the NuA4/TIP60 complex *in vivo* (Figure 3F). Thus, the preceding results validated the physiological significance of these key residues of MBTD1 and EPC1 for their association in human cell lines.

Functional Implications of Uncoupling MBTD1 from the NuA4/TIP60 Acetyltransferase Complex

MBTD1 has been found to co-localize with other NuA4/TIP60 complex subunits at the transcription start sites of active genes, affecting their recruitment and thereby regulating gene transcription (Jacquet et al., 2016). We next examined the functional significance of the interaction between MBTD1 and EPC1 on gene transcription. The MBTD1 or EPC1 mutants that impair the complex formation exhibited significantly reduced binding to the *RPSA* gene promoter, a *bone fide* target of the NuA4/TIP60 complex, as measured by chromatin immunoprecipitation (ChIP) assay (Figure 4A). Although a portion of EPC1 is retained, the MBTD1

recruitment is lost, in agreement with its dissociation from the complex. Furthermore, MBTD1 and EPC1 have been suggested to function as putative tumor suppressors (Jacquet et al., 2016). Clonogenic survival analysis revealed that transfected cells expressing EPC1 or MBTD1 mutants displayed less colony growth compared with the empty vector control (Figures 4B, S4A, and S4B). Notably, significantly more colonies were recovered with the MBTD1 mutant versus its wild-type (WT) version, indicating that MBTD1-dependent growth suppression at least partly requires interaction with the NuA4/TIP60 complex. Collectively, these results confirm the physiological significance of the key residues identified in the MBTD1-EPC1 complex structure.

The MBTD1-associated NuA4/TIP60 complex recognizes the H4K20me mark at DSB sites and catalyzes the acetylation of the histone H4 tail and H2AK15 surrounding the sites of broken chromatins (Tang et al., 2013; Jacquet et al., 2016). These DNA damage-signaling events act in concert to favor downstream recruitment of the HR-mediated repair machinery as the choice of DSB repair pathways, blocking at multiple levels the recruitment and retention of the key NHEJ factor 53BP1 to the DSB sites (Jacquet et al., 2016). Given that we have identified the key residues of MBTD1 responsible for its enlistment into the NuA4/TIP60 complex, we aimed to validate these key residues' functional importance in mammalian cells. It was shown that overexpression of WT MBTD1 led to mild increase of the H2AK15ac (acetylation of lysine 15 on histone H2A) signal in MBTD1 knockout cells, whereas overexpression of the MBTD1 mutant failed to produce this effect (Figure S4C). Furthermore, post-gamma-irradiation clonogenic survival analysis demonstrated that complementation of MBTD1 knockout cells (2 different clones; Jacquet et al., 2016) by transfection of a WT MBTD1 expression vector rescues the radiosensitivity of MBTD1 knockout cells (Figure 4C). In contrast, complementation of the MBTD1 knockout cells with the MBTD1 mutant failed to rescue the radiosensitivity of MBTD1 knockout cells (Figure 4C). Interestingly, ectopic expression of MBTD1 seems to also protect WT cells (containing endogenous MBTD1 protein), while the mutant again fails to do so. These results highlight the functional significance of the MBTD1-EPC1 interactions in repairing damaged chromatin in mammalian cells.

Because MBT1 is important for proper expression of specific genes, directly bound by the NuA4/TIP60 complex or indirectly, we next investigated whether WT MBTD1, but not the mutant lacking the EPC1 binding ability, rescues the gene regulation defects in MBTD1 knockout cells. The expression levels of *HIST1H4C* and *CCDN3* have been shown to be dysregulated in opposite manners in the MBTD1 knockout cells; *HIST1H4C* is overexpressed, whereas *CCDN3* is underexpressed (Jacquet et al., 2016). We measured the expression levels of these two genes in the MBTD1 knockout cells transfected with empty vector, WT MBTD1, or mutant vectors by qRT-PCR. *HOXB2* expression is measured as a negative control, because it is not affected by the loss of MBTD1. Complementation of the MBTD1 knockout cells with a WT MBTD1 vector rescued their transcription defects, significantly decreasing the expression of *HIST1H4C* while increasing the expression of *CCDN3* (Figure 4D). In contrast, the MBTD1 mutant failed to rescue the misregulation of *HIST1H4C* and *CCDN3* even as it was expressed at similar levels compared with the WT vector (Figures 4D and S4D). Thus, the preceding findings validated the key role of the MBTD1-EPC1 interactions in transcriptional regulation mediated by the NuA4/TIP60 acetyltransferase complex.

In brief, our study has elucidated the molecular mechanism by which MBTD1 is enrolled into the dynamic NuA4/TIP60 acetyltransferase complex to regulate transcription and DNA repair pathway choice. These findings will provide information for the development of inhibitors for selectively dissociating MBTD1 from the NuA4/TIP60 acetyltransferase complex, which can have important clinical implications. Drug-induced disruption of the MBTD1 interaction with NuA4/TIP60 could be used to sensitize cancer cells to radiotherapy, alone or in combination with poly (ADP-ribose) polymerase (PARP) inhibitors. This approach may be better than direct inhibition of Tip60 histone acetyltransferase activity, which can lead to larger side effects on healthy cells.

STAR★METHODS

Detailed methods are provided in the online version of this paper and include the following:

- KEY RESOURCES TABLE
- LEAD CONTACT AND MATERIALS AVAILABILITY
- EXPERIMENTAL MODEL AND SUBJECT DETAILS
- METHOD DETAILS
  - Protein expression and purification
  - Crystallization, data collection and structure determination
  - GST pull-down
  - Isothermal titration calorimetry
  - Generation of isogenic cell lines and affinity purification of complexes
  - ChIP-qPCR Assay
  - Clonogenic growth assay
  - Gamma-irradiation and clonogenic survival assay
  - Chromatin extracts
  - Reverse Transcription-qPCR
- QUANTIFICATION AND STATISTICAL ANALYSIS
- DATA AND CODE AVAILABILITY

SUPPLEMENTAL INFORMATION

Supplemental Information can be found online at https://doi.org/10.1016/j.celrep.2020.03.003.

ACKNOWLEDGMENTS

We are grateful to Amelie Fradet-Turcotte for help with the radiosensitivity clonogenic assays. Diffraction data were collected at the Advanced Photon Source of the Argonne National Laboratory. The Structural Genomics Consortium (SGC) is a registered charity (number 1097737) that receives funds from AbbVie; Bayer Pharma AG; Boehringer Ingelheim; the Canada Foundation for Innovation; the Eshelman Institute for Innovation; Genome Canada through the Ontario Genomics Institute (OGI-055); the Innovative Medicines Initiative (EU/EFPIA) (ULTRA-DD grant 115766); Janssen; Merck KGaA; MSD; Novartis Pharma AG; the Ontario Ministry of Research, Innovation and Science (MRIS); Pfizer; the São Paulo Research Foundation (FAPESP); Takeda; and Wellcome. This work was also supported by the Canadian

Institutes of Health Research (CIHR) (FDN-143314 to J.C.) and the Natural Sciences and Engineering Research Council of Canada (NSERC) (RGPIN-2016-06300 to J.M.). J.C. holds the Canada Research Chair in Chromatin Biology and Molecular Epigenetics.

AUTHOR CONTRIBUTIONS

H.Z., M.D., J.C., and J.M. designed the research. H.Z., M.D., X.S., G.A., H.C., W.T., C.D., and P.L. performed experiments. H.Z., M.D., L.L., J.C., and J.M. wrote the manuscript.

DECLARATION OF INTERESTS

The authors declare no competing interests.

Received: June 9, 2019
Revised: January 1, 2020
Accepted: February 28, 2020
Published: March 24, 2020

REFERENCES

Alfieri, C., Gambetta, M.C., Matos, R., Glatt, S., Sehr, P., Fraterman, S., Wilm, M., Müller, J., and Müller, C.W. (2013). Structural basis for targeting the chromatin repressor Sfmbt to Polycomb response elements. Genes Dev. *27*, 2367–2379.

Chapman, J.R., Taylor, M.R., and Boulton, S.J. (2012). Playing the end game: DNA double-strand break repair pathway choice. Mol. Cell *47*, 497–510.

Chen, V.B., Arendall, W.B., 3rd, Headd, J.J., Keedy, D.A., Immormino, R.M., Kapral, G.J., Murray, L.W., Richardson, J.S., and Richardson, D.C. (2010). MolProbity: all-atom structure validation for macromolecular crystallography. Acta Crystallogr. D Biol. Crystallogr. *66*, 12–21.

Chin, J.W. (2017). Expanding and reprogramming the genetic code. Nature *550*, 53–60.

Dalvai, M., Loehr, J., Jacquet, K., Huard, C.C., Roques, C., Herst, P., Côté, J., and Doyon, Y. (2015). A Scalable Genome-Editing-Based Approach for Mapping Multiprotein Complexes in Human Cells. Cell Rep. *13*, 621–633.

Dantuma, N.P., and van Attikum, H. (2016). Spatiotemporal regulation of posttranslational modifications in the DNA damage response. EMBO J. *35*, 6–23.

Dhar, S., Gursoy-Yuzugullu, O., Parasuram, R., and Price, B.D. (2017). The tale of a tail: histone H4 acetylation and the repair of DNA breaks. Philos. Trans. R. Soc. Lond. B Biol. Sci. *372*, 20160284.

Emsley, P., Lohkamp, B., Scott, W.G., and Cowtan, K. (2010). Features and development of Coot. Acta Crystallogr. D Biol. Crystallogr. *66*, 486–501.

Eryilmaz, J., Pan, P., Amaya, M.F., Allali-Hassani, A., Dong, A., Adams-Cioaba, M.A., Mackenzie, F., Vedadi, M., and Min, J. (2009). Structural studies of a four-MBT repeat protein MBTD1. PLoS ONE *4*, e7274.

Evans, P.R., and Murshudov, G.N. (2013). How good are my data and what is the resolution? Acta Crystallogr. D Biol. Crystallogr. *69*, 1204–1214.

Fradet-Turcotte, A., Canny, M.D., Escribano-Díaz, C., Orthwein, A., Leung, C.C.Y., Huang, H., Landry, M.C., Kitevski-LeBlanc, J., Noordermeer, S.M., Sicheri, F., and Durocher, D. (2013). 53BP1 is a reader of the DNA-damage-induced H2A Lys 15 ubiquitin mark. Nature *499*, 50–54.

Gupta, A., Hunt, C.R., Chakraborty, S., Pandita, R.K., Yordy, J., Ramnarain, D.B., Horikoshi, N., and Pandita, T.K. (2014). Role of 53BP1 in the regulation of DNA double-strand break repair pathway choice. Radiat. Res. *181*, 1–8.

Gwak, J., Shin, J.Y., Lee, K., Hong, S.K., Oh, S., Goh, S.H., Kim, W.S., and Ju, B.G. (2016). SFMBT2 (Scm-like with four mbt domains 2) negatively regulates cell migration and invasion in prostate cancer cells. Oncotarget *7*, 48250–48264.

Her, J., and Bunting, S.F. (2018). How cells ensure correct repair of DNA double-strand breaks. J. Biol. Chem. *293*, 10502–10511.

Hustedt, N., and Durocher, D. (2016). The control of DNA repair by the cell cycle. Nat. Cell Biol. *19*, 1–9.

Jacquet, K., Fradet-Turcotte, A., Avvakumov, N., Lambert, J.P., Roques, C., Pandita, R.K., Paquet, E., Herst, P., Gingras, A.C., Pandita, T.K., et al. (2016). The TIP60 Complex Regulates Bivalent Chromatin Recognition by 53BP1 through Direct H4K20me Binding and H2AK15 Acetylation. Mol. Cell *62*, 409–421.

Kabsch, W. (2010). Xds. Acta Crystallogr. D Biol. Crystallogr. *66*, 125–132.

Kee, H.J., Kim, J.-R., Nam, K.-I., Park, H.Y., Shin, S., Kim, J.C., Shimono, Y., Takahashi, M., Jeong, M.H., Kim, N., et al. (2007). Enhancer of polycomb1, a novel homeodomain only protein-binding partner, induces skeletal muscle differentiation. J. Biol. Chem. *282*, 7700–7709.

Lechtenberg, B.C., Allen, M.D., Rutherford, T.J., Freund, S.M., and Bycroft, M. (2009). Solution structure of the FCS zinc finger domain of the human polycomb group protein L(3)mbt-like 2. Protein Sci. *18*, 657–661.

Liu, T., and Huang, J. (2016). DNA End Resection: Facts and Mechanisms. Genomics Proteomics Bioinformatics *14*, 126–130.

Liu, M., Wang, H., Lee, S., Liu, B., Dong, L., and Wang, Y. (2016). DNA repair pathway choice at various conditions immediately post irradiation. Int. J. Radiat. Biol. *92*, 819–822.

Murshudov, G.N., Skubák, P., Lebedev, A.A., Pannu, N.S., Steiner, R.A., Nicholls, R.A., Winn, M.D., Long, F., and Vagin, A.A. (2011). REFMAC5 for the refinement of macromolecular crystal structures. Acta Crystallogr. D Biol. Crystallogr. *67*, 355–367.

Paquin, K.L., and Howlett, N.G. (2018). Understanding the Histone DNA Repair Code: H4K20me2 Makes Its Mark. Mol. Cancer Res. *16*, 1335–1345.

Pommier, Y., Sun, Y., Huang, S.N., and Nitiss, J.L. (2016). Roles of eukaryotic topoisomerases in transcription, replication and genomic stability. Nat. Rev. Mol. Cell Biol. *17*, 703–721.

Rossetto, D., Truman, A.W., Kron, S.J., and Côté, J. (2010). Epigenetic modifications in double-strand break DNA damage signaling and repair. Clin. Cancer Res. *16*, 4543–4552.

Soria, G., Polo, S.E., and Almouzni, G. (2012). Prime, repair, restore: the active role of chromatin in the DNA damage response. Mol. Cell *46*, 722–734.

Sunada, S., Nakanishi, A., and Miki, Y. (2018). Crosstalk of DNA double-strand break repair pathways in poly(ADP-ribose) polymerase inhibitor treatment of breast cancer susceptibility gene 1/2-mutated cancer. Cancer Sci. *109*, 893–899.

Sung, P. (2018). Introduction to the Thematic Minireview Series: DNA double-strand break repair and pathway choice. J. Biol. Chem. *293*, 10500–10501.

Tang, J., Cho, N.W., Cui, G., Manion, E.M., Shanbhag, N.M., Botuyan, M.V., Mer, G., and Greenberg, R.A. (2013). Acetylation limits 53BP1 association with damaged chromatin to promote homologous recombination. Nat. Struct. Mol. Biol. *20*, 317–325.

Tezel, G., Shimono, Y., Murakumo, Y., Kawai, K., Fukuda, T., Iwahashi, N., and Takahashi, M. (2002). Role for O-glycosylation of RFP in the interaction with enhancer of polycomb. Biochem. Biophys. Res. Commun. *290*, 409–414.

Wilson, M.D., and Durocher, D. (2017). Reading chromatin signatures after DNA double-strand breaks. Philos. Trans. R. Soc. Lond. B Biol. Sci. *372*, 20160280.

Woodsmith, J., and Stelzl, U. (2014). Studying post-translational modifications with protein interaction networks. Curr. Opin. Struct. Biol. *24*, 34–44.

Woodsmith, J., Kamburov, A., and Stelzl, U. (2013). Dual coordination of post translational modifications in human protein networks. PLoS Comput. Biol. *9*, e1002933.

Zimmermann, M., and de Lange, T. (2014). 53BP1: pro choice in DNA repair. Trends Cell Biol. *24*, 108–117.

STAR★METHODS

KEY RESOURCES TABLE

REAGENT or RESOURCE	SOURCE	IDENTIFIER
Bacterial and Virus Strains		
BL21-CodonPlus (DE3)-RIL	Agilent Technologies	Cat# 230245
Biological Samples		
RPMI	GIBCO	Cat# 21870-076
DMEM	GIBCO	Cat# 11995-065
New Born Calf serum	Multicell Technologies	Cat# 075150
Fetal Bovine serum	GIBCO	Cat# 12483-020
Chemicals, Peptides, and Recombinant Proteins		
SYBR Green I	Roche	Cat# 03003230001
Crystal violet	Sigma-Aldrich	Cat# C6158
Tobacco Etch Virus (TEV) protease	Homemade	N/A
Protease Inhibitor Cocktail	Sigma-Aldrich	Cat# P8340
Lipofectamine 2000	Invitrogen	Cat# 11668-019
Rneasy Mini kit	QIAGEN	Cat# 74104
qScprit cDNA Supermix kit	VWR	Cat# CA101414-098
GlutaMax-I supplement	Thermo fisher scientific	Cat# 35050-061
Puromycin dihydrochloride	Life Technologies	Cat# A1113802
Anti-H2AK15ac antibody	Abcam	Cat# ab101447; RRID:AB_10710543
Anti-H3 antibody	Abcam	Cat# ab1791; RRID:AB_302613
Anti-H4 antibody	Abcam	Cat# Ab7311;RRID:AB_305837
Anti-H4 penta-acetyl antibody	Upstate	Cat# 06-946; RRID:AB_11213428
Anti-MBTD1 antibody	Abcam	Cat# ab116361; RRID:AB_10899589
Anti-GST antibody	Sigma	Cat# G1160; RRID:AB_259845
Anti-Tip60 antibody	Abcam	Cat# ab137518
Anti-IgG antibody	Millipore	Cat# PP64; RRID:AB_97852
Anti-GAPDH antibody	Thermo fisher scientific	Cat#39-8600; RRID:AB_2533438
Anti-FLAG M2-Peroxidase (HRP) antibody	Sigma-Aldrich	Cat# A8592; RRID:AB_439702
Anti-Flag M2 antibody	Sigma-Aldrich	Cat# F1804; RRID:AB_262044
3x FLAG peptide	Sigma-Aldrich	Cat# F4799
Critical Commercial Assays		
Ni-NTA agarose resin	QIAGEN	Cat# 30430
Glutathione Agarose	Thermo fisher scientific	Cat# 16100
Dynabeads protein G	Invitrogen	Cat# 10004D
ANTI-FLAG M2 Affinity Gel	Sigma-Aldrich	Cat# A2220
Deposited Data		
MBTD1-EPC1 structure	This study	PDB: 6NFX
Experimental Models: Cell Lines		
U2OS	(Jacquet et al., 2016)	ATCC HTB-96
K562	(Jacquet et al., 2016)	ATCC CCL-243
pAAVS1-3xFlag2xStrep-EPC1 WT	(Dalvai et al., 2015)	N/A
pAAVS1-3xFlag2xStrep-EPC1 $^{1-464}$	This paper	N/A
pAAVS1-3xFlag2xStrep-EPC1 $^{L651D/A660D/L663D}$	This paper	N/A
pAAVS1-3xFlag2xStrep-MBTD1 WT	This paper	N/A

(*Continued on next page*)

Continued

REAGENT or RESOURCE	SOURCE	IDENTIFIER
pAAVS1-3xFlag2xStrep-MBTD1 $^{A236D/L259D/L263D}$	This paper	N/A
Recombinant DNA		
pET28-MHL-MBTD1-EPC1	This paper	N/A
pET28-MHL-MBTD1	This paper	N/A
pET28GST-LIC-EPC1	This paper	N/A
Software and Algorithms		
PyMOL	Schrodinger LLC	https://pymol.org/2/
Coot	(Emsley et al., 2010)	https://www2.mrc-lmb.cam.ac.uk/personal/pemsley/coot/
XDS	(Kabsch, 2010)	http://xds.mpimf-heidelberg.mpg.de
AIMLESS	(Evans and Murshudov, 2013)	N/A
REFMAC	(Murshudov et al., 2011)	N/A
MOLPROBITY	(Chen et al., 2010)	http://molprobity.biochem.duke.edu/

LEAD CONTACT AND MATERIALS AVAILABILITY

Further contact information and requests for resources and reagents should be directed to and will be fulfilled by the Lead Contact, Jinrong Min (jr.min@utoronto.ca). This study did not generate new unique reagents.

EXPERIMENTAL MODEL AND SUBJECT DETAILS

The plasmid DNAs were amplified in *E. coli* DH5α cells. MBTD1 and EPC1 proteins were expressed in *E. coli* BL21-CodonPlus (DE3)-RIL cells cultured at 37°C or 18°C in TB medium. K562 and U2OS cells were obtained from the ATCC and maintained at 37°C under 5% CO2. K562 were cultured in RPMI medium supplemented with 10% newborn calf serum and GlutaMAX. U2OS cells were cultured in DMEM medium supplemented with 10% fetal bovine serum.

METHOD DETAILS

Protein expression and purification

The MBTD1$^{140–562}$-$(GSA)_6$-EPC1$^{644–672}$ fusion protein construct was cloned into the pET28-MHL vector. Recombinant proteins were expressed in *E. coli* strain BL21-CodonPlus (DE3)-RIL in TB medium overnight at 16°C. Cells were collected by centrifugation at 4°C and resuspended in 25 mM Tris–HCl pH 8.0, 500 mM NaCl, 5 mM β-mercaptoethanol, 1 mM PMSF. Subsequently, cells were lysed by sonication and debris was removed by centrifugation at 4°C. The supernatants were loaded onto a Ni-NTA resin (QIAGEN) gravity column and eluted with buffer containing 25 mM Tris-HCl pH 8.0, 500 mM NaCl, 250 mM imidazole, 5 mM β-mercaptoethanol. The proteins were further purified by anion-exchange chromatography and subsequent gel-filtration chromatography in a buffer containing 25 mM Tris-HCl pH 8.0, 150 mM NaCl. Peak fractions were concentrated to 16 mg/mL.

Crystallization, data collection and structure determination

Co-crystallization trials of purified MBTD1$^{140–562}$ and EPC1$^{644-672}$ proteins were not successful. Thus, we generated a fusion construct in which EPC1$^{644-672}$ was C-terminally linked to MBTD1$^{140–562}$ using a $(GSA)_6$ linker. Remarkably, the MBTD1-EPC1 fusion protein yielded high-quality crystals that diffracted to a resolution of 1.9 Å and enabled us to solve the complex structure. Crystal screening was performed by sitting-drop vapor-diffusion at 18 °C. Crystals of MBTD1-EPC1 were obtained using a reservoir solution composed of 0.1 M sodium citrate tribasic dihydrate pH 5.0, 10% w/v polyethylene glycol 6,000. The crystals were soaked in a cryo-protectant of crystallization solution supplemented with 20% glycerol before being flash-frozen. Diffraction data were collected at beam line 19-ID of the Advanced Photon Source and reduced with XDS (Kabsch, 2010) and AIMLESS (Evans and Murshudov, 2013). The structure was solved by molecular replacement with coordinates from PDB entry 3FEO (Eryilmaz et al., 2009). The model was iteratively refined with REFMAC (Murshudov et al., 2011) and rebuilt with COOT (Emsley et al., 2010). Model geometry was evaluated with MOLPROBITY (Chen et al., 2010).

GST pull-down

EPC1 fragments with the indicated boundaries were cloned into the pET28GST-LIC vector that encodes an N-terminal GST-tag. All point mutations were generated using the Quick Change Site–directed mutagenesis system (Stratagene, La Jolla, CA). All

GST-tagged proteins were expressed in BL21(DE3) cells and purified by GST affinity chromatography (Glutathione agarose). Proteins were then dialyzed overnight against dialysis buffer (25 mM Tris-HCl, pH 8.0, 150 mM NaCl, 1 mM β-mercaptoethanol). The GST-tagged proteins were first incubated with glutathione resin for 1 hour at 4°C in dialysis buffer. His-tagged MBTD1 proteins were incubated with the beads for 30 min at 4°C. The samples were washed four times with 1 mL dialysis buffer to remove excess unbound protein, and then analyzed through Coomassie staining of SDS-PAGE or western blotting. Anti-MBTD1 (Abcam Ab116361) antibodies were used for western blotting at 1:1000 dilution.

Isothermal titration calorimetry

Proteins were expressed and purified as described above. The ITC experiments were performed on a Microcal VP-ITC (Microcal, Amherst, MA) at 25 °C. All measurements were carried out at a stirring speed of 307 rpm, in 25 mM Tris-HCl, pH 8.0, 150 mM NaCl. For H4K20me1 binding assay, the H4K20me1 peptide (1 mM) was titrated into the MBTD1 or MBTD1-EPC1 fusion protein solution (10 μM) with 26 injections. For the MBTD1-EPC1 binding assay, each titration was carried out by injecting the EPC1 WT or mutants proteins (0.2 mM) into the cell containing MBTD1 WT or mutants proteins (10 μM). The ITC experiments were repeated at least two times. The binding data were subsequently analyzed using Origin (MicroCal).

Generation of isogenic cell lines and affinity purification of complexes

K562 cells were used to express various 3xFlag-tagged EPC1 proteins including EPC1 WT, EPC1$^{1\text{-}464}$, EPC1$^{L651D/L663D}$, and EPC1$^{L651D/A660D/L663D}$ as well as 3xFlag-tagged MBTD1 WT and MBTD1$^{A236D/L259D/L263D}$ from the AAVS1 safe harbor using ZFN-mediated insertion as described previously (Dalvai et al., 2015). After whole cell extraction, anti-Flag immunoprecipitation was performed with anti-FLAG agarose affinity gel (Sigma M2), followed by elution with 3xFLAG peptide (200 μg/ml from Sigma in the following buffer: 20 mM HEPES pH7.9, 100 mM KCl, 0.1% Triton X-100, 20% glycerol, 100 μM $ZnCl_2$, 1 mM DTT and supplemented with proteases, deacetylases and phosphatases inhibitors).

Flag eluates from the above preparations were normalized following SDS-PAGE and transfer onto a nitrocellulose membrane. The following antibodies were used at the indicated dilution: anti-FLAG-HRP conjugate (Sigma M2, 1:5000), anti-Tip60 (Abcam 137518, 1:1000); anti-MBTD1 (Abcam ab116361, 1:1000); anti-GAPDH (ThermoFisher, 39-8600, 1:10000).

ChIP-qPCR Assay

For anti-FLAG ChIP, 1 mg of cross-linked chromatin from K562 cells was incubated with 10 μg of anti-FLAG antibody (Sigma, M2) or anti-IgG antibody (Millipore- PP64) pre-bound on 300 μl of Dynabeads Prot-G (Invitrogen) overnight at 4°C. The beads were washed extensively and eluted in 0.1% SDS, 0.1 M NaHCO3. Crosslink was reversed with 0.2 M NaCl and incubation overnight at 65°C. Samples were treated with RNase and Proteinase K for 2 h and recovered by phenol chloroform extraction and ethanol precipitation. Quantitative real-time PCRs were performed on a LightCycler 480 (Roche) with SYBR Green I (Roche) to confirm specific enrichment at the RPSA locus. Ratios of immunoprecipitated signal versus input are based on duplicate experiments and errors bars represent the range. Primers used: AGAAAGCGGGCTAACATCCT; GCTGTGCTGTCACCACTTGT.

Clonogenic growth assay

EPC1 WT, EPC1$^{L651D/A660D/L663D}$, MBTD1 WT, MBTD1$^{A236D/L259D/L263D}$ or empty vectors were transfected into U2OS cells which were then seeded onto dishes in duplicates. Subsequently, puromycin [1μg/μl] was added to the culture media at 48hours post-transfection for selection. After ten days of culture, the colonies formed on the dishes were fixed with methanol, followed by staining with crystal violet (Sigma C6158) and washing with distilled water. Images of the dishes were then taken.

Gamma-irradiation and clonogenic survival assay

MBTD1-3xFlag, MBTD1$^{A236D/L259D/L263D}$-3xFlag mutant or an empty vector were transfected into U2OS cells or MBTD1 KO cell lines previously described (Jacquet et al., 2016). Cells were then seeded in 10cm dishes. Puromycin was added to the culture media [1μg/ml] 48hrs post-transfection for two days of selection. One day before irradiation, the cells were counted to plate 500 cells per condition in 6-well plates. Irradiation with 0 or 0.5 gray was performed using a Cellrad Faxitron irradiator. After 12 days of culture, the colonies formed were fixed with methanol, followed by staining with crystal violet (Sigma C6158) and washes with distilled water. Images were then taken, and colonies counted.

Western blot analysis of whole cell extracts from the above transfections were done to verify equivalent expression of WT and mutant proteins. The following antibodies were used at the indicated dilution: anti-FLAG-HRP conjugate (Sigma M2, 1:5000) and anti-GAPDH (ThermoFisher, 39-8600, 1:10000). The error bars represent the range based on independent experiments.

Chromatin extracts

Chromatin-enriched extracts were prepared as described before (Gwak et al., 2016). Briefly, U2OS cells were transfected with WT MBTD1-3xFlag, MBTD1$^{A236D/L259D/L263D}$-3xFlag mutant or an empty vector (4μg) using Lipofectamine 2000. 2 days post-transfection, puromycin was added [1 μg/ml]. 48hrs later cells were harvested, washed once with PBS 1X and resuspended in buffer 1 (50mM Tris-HCl pH7.5, 100mM NaCl, 1mM EDTA, 1mM DTT, 1X protease inhibitor cocktail (Sigma- P8340), 1mM PMSF, 20mM N-ethylmaleimide, 10mM NaB, 10mM NaF). Cell suspension was incubated 5 min on ice, then centrifuged at 1000 g for 15 minutes.

Supernatant was discarded. Nuclei were then resuspended in buffer 2 (50mM Tris-HCl pH7.5, 300mM NaCl, 1mM EDTA, 5mM $CaCl_2$, 1mM DTT, 1X protease inhibitor cocktail, 1mM PMSF), incubated 10 min on ice and sonicated 3x30 s. Chromatin enriched extracts were finally clarified by centrifugation at 1000 g for 20 min. The following antibodies were used for western blotting at the indicated dilution: anti-H2AK15ac (Abcam ab101447, 1:1000); anti-H4penta-Acetyl (Upstate 06-946, 1:3000); anti-H3 (Abcam 1791, 1:10 000); anti-H4 (Abcam 7311, 1:5000).

Reverse Transcription-qPCR

WT MBTD1-3xFlag, MBTD1$^{A236D/L259D/L263D}$-3xFlag mutant or an empty vector were transfected in a MBTD1 KO U2OS cell line (#15; Jacquet et al., 2016). Puromycin [1μg/ml] was added 48hrs post-transfection and 48hrs later total RNA was extracted with the RNeasy Plus Mini kit (QIAGEN). 500 ng of RNA was reverse transcribed by oligo-dT and random priming into cDNA with a qScript cDNA SuperMix kit (QuantaBio-VWR), according to the manufacturer's instructions.

Quantification of the amount of cDNA was done with SYBR Green I (Roche) on a LightCycler 480 (Roche) for real-time PCR, using primers specific for *HIST1H4C* and *CCDN3* coding regions, two genes that are affected in MBTD1 KO cells (Jacquet et al., 2016). The HOXB2 *gene was used* as negative control as it is not affected in MBTD1 KO cells. The *36B4* gene was used as a housekeeping internal control for normalization. The error bars represent the range based on independent experiments. The oligonucleotide sequences used for expression analysis by RT-qPCR are listed below:

Primer name	For	Rev
36B4	CGACCTGGAAGTCCAACTAC	ATCTGCTGCATCTGCTTG
HIST1H4C	ATCCAGGGCATTACAAAACCG	AACCTTAAGCACACCTCGAGT
CCDN3	GGAAGATGCTGGCTTACTGGA	GACAGGTAGCGATCCAGGTAG
HOXB2	TAATAAGTACCTGTGCCGGCC	CTTCATGCGCCGGTTCTGAAA

QUANTIFICATION AND STATISTICAL ANALYSIS

Statistics generated from X-ray crystallography data processing, refinement, and structure validation are displayed in Table S1. ChIP data in Figure 4A are shown as % of input chromatin signal subtract by the IgG background. Clononegic survival assay in Figures 4B and 4C are shown as the mean of the number of colonies relative to the empty vector of two independent experiments. The Figure 4D represents the mean of the quantification of cDNA of specific genes relative to the housekeeping gene 36B4 of two independent experiments. The error bars of all these figures represent the range.

DATA AND CODE AVAILABILITY

The accession number for the coordinates and structure factors for MBTD1-EPC1 reported in this paper is PDB: 6NFX.